CHEMISTRY

A EUROPEAN JOURNAL

18/26 2012

A Journal of ChemPubSoc Europe

Supported by ACES

Review

Protein Conformational Switches: From Nature to Design

S. N. Loh and J.-H. Ha

WILEY-VCH

CEUJED 18 (26) 7965–8244 (2012) · ISSN 0947-6539 · Vol. 18 · No. 26 · 2012

www.chemeurj.org

CHEMISTRY
A EUROPEAN JOURNAL

… the first of its kind, derived from a simple organic salt has been demonstrated to be stable for months. The same gel also showed remarkable load-bearing and self-healing properties. A crystal engineering approach was adopted to discover such wonderful soft material. For more details, see the Full Paper by P. Dastidar et al. on page 8057 ff.

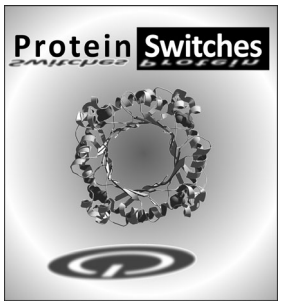

Protein Engineering
Proteins are unique in nature in that they incorporate a large array of conformational change modes into an equally diverse repertoire of biological functions. Cells and viruses employ protein conformational switches for molecular recognition, environmental sensing, and regulating signaling pathways involved in development, homeostasis, immunity, infection, and other cellular processes. Structural and biochemical elucidation of some of these switching mechanisms has enabled researchers to begin adapting them for use in biosensing and functional regulation. For more details see the Review by S. N. Loh and J.-H. Ha on page 7984 ff.

Coordination Polymers
In their Communication on page 8013 ff., J. A. Real et al. report a new Fe^{II} spin crossover porous coordination polymer, $\{Fe(dpe)[Pt(CN)_4]\}$, that functions as a robust host cage for reversible encapsulation of aromatic compounds. Detection of the guest molecules was performed by analyzing the temperature dependence of the magnetic susceptibility of the corresponding clathrate. A fingerprint-like magnetic response pattern to each analyte was attained.

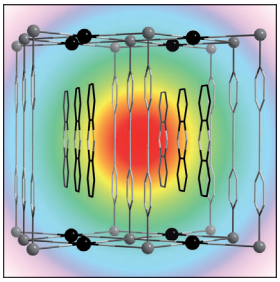

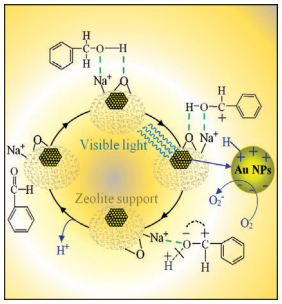

Gold Nanoparticles
Gold nanoparticles (Au-NPs) can absorb visible light due to as surface plasmon resonance effect and selectively oxidize aromatic alcohols at ambient temperature. In such photooxidation reactions, the interaction between aromatic alcohols and zeolite contributes to enhance the local electromagnetic field of incident light. More importantly, the photooxidation of benzyl alcohol significantly reduced the apparent activation energy compared with thermal-activation oxidation. The finding may inspire further studies on various organic syntheses driven by sunlight, design of new photocatalysts, catalytic reaction mechanism, and green chemistry processes. For more details see the Full Paper by X.-B. Ke et al. on page 8048 ff.

CHEMISTRY
A EUROPEAN JOURNAL

FULL PAPER

DOI: 10.1002/chem.201200986

Gel Sculpture: Moldable, Load-Bearing and Self-Healing Non-Polymeric Supramolecular Gel Derived from a Simple Organic Salt

Pathik Sahoo,[a] Ravish Sankolli,[b] Hee-Young Lee,[c] Srinivasa R. Raghavan,[c] and Parthasarathi Dastidar*[a]

Abstract: An easy access to a library of simple organic salts derived from *tert*-butoxycarbonyl (Boc)-protected L-amino acids and two secondary amines (dicyclohexyl- and dibenzyl amine) are synthesized following a supramolecular synthon rationale to generate a new series of low molecular weight gelators (LMWGs). Out of the 12 salts that we prepared, the nitrobenzene gel of dicyclohexylammonium Boc-glycinate (**GLY.1**) displayed remarkable load-bearing, moldable and self-healing properties. These remarkable properties displayed by **GLY.1** and the inability to display such properties by its dibenzylammonium counterpart (**GLY.2**) were explained using microscopic and rheological data. Single crystal structures of eight salts displayed the presence of a 1D hydrogen-bonded network (HBN) that is believed to be important in gelation. Powder X-ray diffraction in combination with the single crystal X-ray structure of **GLY.1** clearly established the presence of a 1D hydrogen-bonded network in the xerogel of the nitrobenzene gel of **GLY.1**. The fact that such remarkable properties arising from an easily accessible (salt formation) small molecule are due to supramolecular (non-covalent) interactions is quite intriguing and such easily synthesizable materials may be useful in stress-bearing and other applications.

Keywords: crystal engineering · gels · gelators · X-ray diffraction · supramolecular chemistry

Introduction

Materials that can be molded to form self-supporting, shape-persistent objects are of great importance in materials science and technology.[1] Self-healing is another highly sought-after material property that is usually seen in naturally occurring materials such as bone, wood, biological tissues.[2] Self-healing materials are of great importance as they offer longer lifetime, low replacement cost and greater product safety and can be used in any stress-bearing applications. Chemically cross-linked synthetic hydrogels[3] do not possess self-healing properties and are often found to be brittle. Self-healing requires an energy dissipation process that involves reversibly breakable cross-links with finite lifetimes.[4] This can be achieved through non-covalent interactions rather than through permanent covalent cross-links.[5] Although moldability or plasticity is a well-studied property of thermoplastic polymers, synthetic materials that possess both moldablity and self-healing properties are not so common. Most of the materials displaying both moldablity and self-healing properties reported thus far are hydrogels derived from polymers and nanoparticles such as clays.[1,5]

To our knowledge, supramolecular organogels derived from low molecular weight gelators (LMWGs) displaying both moldablity and self-healing are extremely rare.[6] LMWGs[7,8] are small organic compounds (typically with molecular weights <3000) capable of immobilizing (gelling) large amounts of solvent. The resultant solid-like materials (gels) are being investigated with vigor owing to their various possibilities for application.[9–12] However, designing gelators is a daunting task. Serendipity plays a major role in gel science and most gelators have been found by an accident rather than by design. Nevertheless, there are some efforts to design gelators.[13] In all these attempts, the target gelator molecule is obtained through time-consuming and complex organic synthesis, which often leads to frustration in the quest for new LMWGs. Our approach towards the design of LMWGs, on the other hand, has been based on the supramolecular synthon.[14] By exploiting this strategy, it is possible to generate a supramolecular assembly of various dimensions (1D, 2D or 3D). Microscopic (optical, scanning electron, transmission electron, atomic force, confocal etc.)

[a] P. Sahoo, Dr. P. Dastidar
Department of Organic Chemsitry
Indian Association for the Cultivation of Science (IACS)
2A and 2B, Raja S. C. Mullick Road
Jadavpur, Kolkata - 700032, West Bengal (India)
Fax: (+91) 33-2473-2805
E-mail: ocpd@iacs.res.in
parthod123@rediffmail.com

[b] R. Sankolli
SSCU, Indian Institute of Science
Bangalore - 560012 (India)

[c] Dr. H.-Y. Lee, Prof. Dr. S. R. Raghavan
Department of Chemical & Biomolecular Engineering
University of Maryland, College Park
MD 20742-2111 (USA)

Supporting information for this article is available on the WWW under http://dx.doi.org/10.1002/chem.201200986.

studies on gel/xerogel (dried gel) samples reveal the existence of networks of highly branched and/or entangled 1D fibers, which are known as self-assembled fibrillar networks (SAFINs).[15] The solvent molecules are immobilized within the SAFINs, resulting in gels. The entangled 1D fiber or SAFIN formation may be attributed to some anisotropic interactions that help the gelator molecules preferentially self-assemble in 1D, whereas the lack of such interactions in the other two dimensions prevents lateral growth. Thus, molecules that have self-complementary, reasonably strong, and directional hydrogen bonding site(s) are expected to form 1D fibers which ultimately might lead to SAFINs. This hypothesis originally proposed by Shinkai and co-workers[16] has been most explicitly demonstrated by us—we used the supramolecular synthon concept to identify a number of organic salts that have the ability to undergo 1D growth, and we were able to confirm that these molecules acted as gelling agents.[7,17]

Among the various organic-salt-based supramolecular synthons that we identified and exploited in designing LMWGs, the secondary ammonium monocarboxylate (**SAM**) synthon is particularly interesting. **SAM** salts display both 1D and 0D (discrete) synthons (synthon A and B, respectively, Scheme 1). The dimensionality of the **SAM**

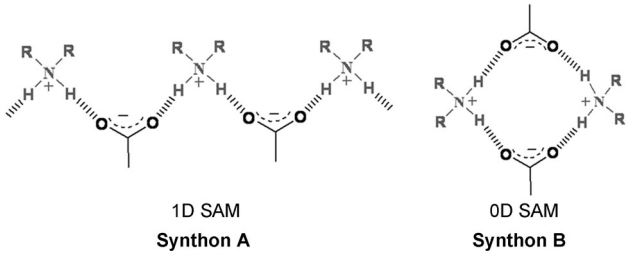

Scheme 1. 1D HBN formation of synthon A, and 0D HBN formation of synthon B.

supramolecular synthon was shown to be dependent on both the cation and the anion. For example, the cinnamate salts of dicyclohexylamine corresponded to a 1D synthon (synthon A), whereas the corresponding benzoate salts resulted in a 0D synthon (synthon B) HBN in the single crystal structures.[17] However, when a dibenzylammonium cation was used, most of the cinnamate and benzoate salts displayed a 1D synthon A.[18] Hydrogen bond isomerism (0D to 1D) was also observed in the dicyclohexylammonium salts of alkyl monocarboxylic acids.[19] About 34% of the **SAM** salts that we have reported thus far[17–22] showed moderate to good gelation properties; all the 18 gelator salts for which single crystal structures could be obtained showed 1D synthon A exclusively, whereas among the 33 single crystal structures of the non-gelator **SAM** salts reported by us, 23 salts showed 0D synthon B, 8 salts displayed 1D synthon A and 2 salts showed a halogen···halogen interaction assisted 2D network. These results demonstrate the efficiency of the **SAM** synthon and the importance of 1D HBN in gelation.

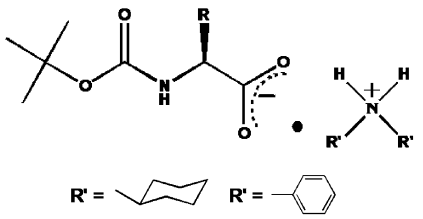

GLY.1: R = H;	**GLY.2**: R = H;
ALA.1: R = Me;	**ALA.2**: R = Me;
VAL.1: R = *i*Pr	**VAL.2**: R = *i*Pr
LEU.1: R = *i*Bu	**LEU.2**: R = *i*Bu
ILE.1: R = 2°Bu	**ILE.2**: R = 2°Bu
PHE.1: R= CH_2Ph	**PHE.2**: R= CH_2Ph

Scheme 2. Boc-protected L-amino acids were treated with two secondary amines to generate the **SAM** salts.

In this article, we present a series of simple **SAM** salts (Scheme 2), some of which displayed organogelation properties. Particularly remarkable is the salt **GLY.1**; the nitrobenzene gel of **GLY.1** showed moldable, load-bearing, and self-healing properties. The moldablity of nitrobenzene gel of **GLY.1** was so impressive that it allowed us to create a sculpture of "mother and child" ($\approx$4.0 inches in height, weighing $\approx$158.0 g) that has remained stable for months (see below). To our knowledge, such properties have not been previously observed for an organogel derived from such a simple organic salt.

Results and Discussion

Synthesis: Commercially obtained *tert*-butoxycarbonyl (Boc)-protected L-amino acids were treated with the corresponding amines, namely dicyclohexylamine (DCHA) or dibenzylamine (DBA) in a 1:1 molar ratio in MeOH at room temperature. After evaporation of the solvent in a rotary evaporator, the white precipitate obtained in near quantitative yield was washed with hexane to remove unreacted amine. ^{1}H NMR spectroscopy and elemental analysis clearly established the stoichiometry of the products as 1:1 (acid/amine). The presence of a strong band within the range of 1612–1651 cm^{-1} in the FTIR spectra indicated salt formation (see the Supporting Information, pages S2 and S3).

Single crystal X-ray diffraction

Supramolecular synthons: To assess the robustness of the **SAM** synthon in these salts, it was necessary to determine the single crystal structures of the salts. We were able to crystallize 8 salts namely **GLY.1, LEU.1**, **PHE.1**, **LEU.2**, **ILE.2**, **GLY.2**, **ALA.2**, and **PHE.2**, out of the 12 salts synthesized. Single crystal X-ray diffraction studies (see the Supporting Information, Table S1) revealed the presence of an overall 1D hydrogen-bonded network in the crystal structures of these salts. More detailed analyses of the crystal

structures indicated the presence of three different types of 1D HBNs.

*Crystal structures of dicyclohexyammonium Boc-glycinate (GLY.1)—double-stranded 1D **SAM** synthon*: The salt **GLY.1** crystallizes in the centrosymmetric triclinic space group $P\bar{1}$. One ion pair is located in the asymmetric unit. FTIR data (1645 cm^{-1} attributed to COO^-) and the C–O distances of the carboxylic moiety [1.2514(17)–1.2554(17) Å] indicate salt formation. A typical 1D **SAM** synthon is observed, involves N–H···O interactions (N···O = 2.6998(15)–2.7081(16) Å; ∡ N–H···O = 171.9–174.0°). However, such 1D chains are self-assembled to form a 1D double-stranded tape sustained by N–H···O interactions (N···O = 2.9289(16) Å; ∡ N–H···O = 154.4°; Figure 1 and the Supporting Information, Table S2 and Figure S1).

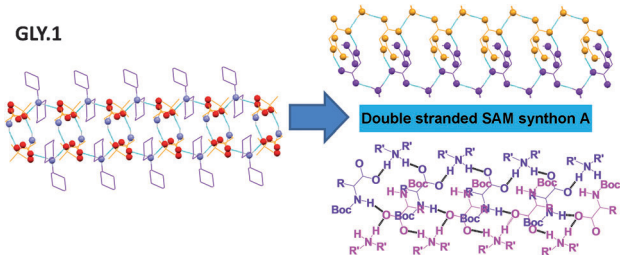

Figure 1. Left: 1D hydrogen-bonded network in the crystal structures of **GLY.1**. Right: existence of 1D double stranded **SAM** synthon A in **GLY.1** and its schematic representation (the side chain of the amino acid and the ammonium cation are hidden for better clarity).

*Crystal structures of dicyclohexyammonium Boc-leucinate (**LEU.1**) and dicyclohexylammonium Boc-phenylalaninate (**PHE.1**)—A typical 1D **SAM** synthon*: The salts **LEU.1** and **PHE.1** are isomorphous and have the same noncentrosymmetric orthorhombic space group $P2_12_12_1$ and near identical cell dimensions. The asymmetric unit is comprised of one ion pair. Strong bands at 1634 and 1624 cm^{-1} in FTIR and C–O distances of 1.236(4)–1.251(4) Å and 1.246(3)–1.262(3) Å in **LEU.1** and **PHE.1**, respectively, provide evidence of salt formation. In the crystal structures, the cation and the anion are hydrogen bonded through N–H···O interactions (N···O = 2.713(4)–2.743(4) Å; ∡ N–H···O = 167.4–177.2° for **LEU.1**; N···O = 2.700(3)–2.748(3) Å; ∡N–H···O = 157.6–173.1° for **PHE.1**); this results in a 1D infinite chain (synthon A, Scheme 1; Figure 2). The chains are further packed in a parallel fashion and are apparently stabilized by dispersion forces in **LEU.1** and by C–H···π (3.849 Å) interactions involving one of the methylene CH groups of the cyclohexyl moiety and the phenyl ring of the amino acid side chain in **PHE.1** (see the Supporting Information, Tables S5 and S8 and Figures S4 and S7).

*Crystal structures of dibenzylammonium Boc-leucinate (**LEU.2**), dibenzylammonium Boc-isoleucinate (**ILE.2**) and dibenzylammonium Boc-glycinate (**GLY.2**)—1D hydrogen-bonded tape involving **SAM** synthon A*: The salts **LEU.2** and **ILE.2** are isostructural as is evident from their different cell dimensions and identical space group (noncentric monoclinic $P2_1$). The asymmetric unit contains one ion pair. A strong band at 1647 and 1649 cm^{-1} and C–O distances of 1.252(3)–1.254(3) Å and 1.249(3)–1.263(3) Å for **LEU.2** and **ILE.2**, respectively, which clearly supports salt formation. The ion pairs are involved in hydrogen bonding through N–H···O interactions (N···O = 2.678(3)–2.797(4) Å; ∡ N–H···O = 165.6–175.3° in **LEU.2**; N···O = 2.688(3)–2.698(3) Å; ∡N–H···O = 147.9–161.1° in **ILE.2**) resulting in the formation of a 1D infinite chain akin to 1D **SAM** synthon A; the cations and anions are assembled on either side of the chain and the Boc-protected NH is found to be involved in a rather weak hydrogen-bonding interaction with one of the carboxylate O atoms (N···O = 3.085(4) Å; ∡ N–H···O = 166.6° in **LEU.2** and N···O = 3.058(3) Å; ∡N–H···O = 160.8° in **ILE.2**]; thus the overall HBN may be best described as 1D tape running parallel to the *a*-axis (Figure 3). The 1D tapes are packed in a parallel fashion apparently stabilized

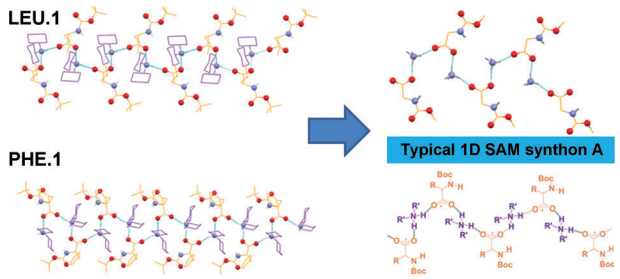

Figure 2. Left: 1D hydrogen-bonded network in the crystal structures of **LEU.1** and **PHE.1**. Right: existence of 1D **SAM** synthon A in these structures (the side chain of the amino acid and the ammonium cation are hidden for better clarity).

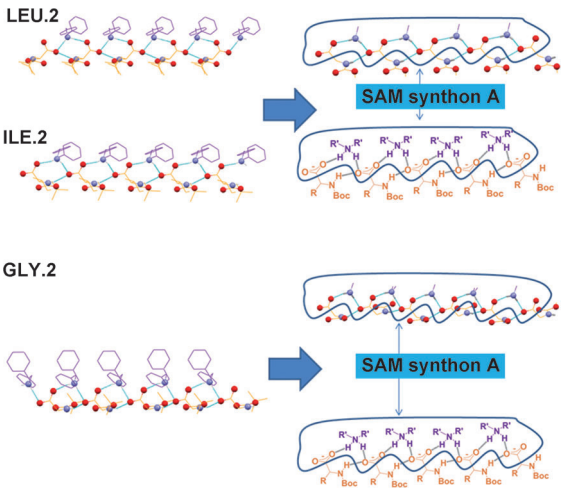

Figure 3. Left: 1D hydrogen-bonded tape in the crystal structures of **LEU.2**, **ILE.2**, and **GLY.2**. Right: details of 1D hydrogen-bonded tape, wherein Boc-protected N–H takes part in hydrogen bonding; the existence of 1D **SAM** synthon A is marked (the side chain of the amino acid and the ammonium cation are hidden for better clarity).

by dispersion forces (see the Supporting Information, Tables S6 and S7 and Figures S5 and S6).

Glycine being an achiral molecule, the salt **GLY.2** crystallized in the centrosymmetric monoclinic space group $P2_1/n$. The asymmetric unit contains one amine and one acid moiety. The C–O distances of 1.253(2)–1.260(2) Å clearly indicate the carboxylate nature of the acid moiety revealing salt formation. The FTIR band at 1629 cm^{-1} also supports salt formation. In the crystal structure, each ammonium cation is hydrogen bonded with the adjacent two carboxylate anions by N–H···O (N···O = 2.692(2)–2.729(2) Å; ∡ N–H···O = 165.2–165.7°) interactions resulting in an infinite 1D chain, as expected for 1D **SAM** synthon A. However, the Boc-protected NH also participates in hydrogen-bonding interactions with one of the O atoms of the adjacent carboxylate anion (N···O = 2.853(2) Å; ∡N–H···O = 149.5°), resulting in a 1D tape-type HBN (see the Supporting Information, Table S3 and Figure S2). Thus, the HBN present in this structure is almost identical to that observed in **LEU.2** and **ILE.2** except that the anionic moieties are arranged in an up and down fashion in an alternating manner, whereas the carboxylate moietes in **LEU.2** and **ILE.2** are located on the same side of the propagating axis of the 1D hydrogen-bonded tape (Figure 3). The 1D tapes are further packed in a parallel fashion apparently stabilized by C–H···π interactions involving the C–H of the methylene group of the amino acid moiety and one of the phenyl rings of the benzyl moiety of the cation (C–H···$\pi_{centroid}$ = 3.640 Å; see the Supporting Information, Tables S6 and S7 and Figures S5 and S6).

*Crystal structure of dibenzylammonium Boc-alaninate (**ALA.2**) and dibenzylammonium Boc-phenylalaninate (**PHE.2**)—1D hydrogen bonded tape involving synthon B*: The single crystals of **ALA.2** and **PHE.2** belong to the non-centrosymmetric space groups $P1$ (triclinic) and $P2_12_12_1$ (orthorhombic), respectively. In the asymmetric units of both the salts, two cations and two anions are located. The C–O distances of 1.206(9)–1.242(9) Å in **ALA.2** and 1.203(3)–1.253(10) Å in **PHE.2** indicate the deprotonation of the acid group, and this was also supported by FTIR (1612 and 1625 cm^{-1} for **ALA.2** and **PHE.2**, respectively). The ion pairs are involved in N–H···O hydrogen-bonding interactions involving the ammonium NH and carboxylate O atoms resulting in the discrete assembly akin to the **SAM** synthon B; in **ALA.2**, one of the ammonium H atoms participates in bifurcated hydrogen-bonding interactions with the carboxylate O atoms, that are not present in **PHE.2**. Such discrete HBNs are further self-assembled to form a 1D hydrogen-bonded tape stabilized by N–H···O interactions (N···O = 2.660(9)–2.901(9) Å; ∡N–H···O = 130.8–165.5° in **ALA.2**; N···O = 2.902(3)–2.995(2) Å; ∡ N–H···O = 153.3–156.0° in **PHE.2**) involving the Boc-protected NH and carboxylate moieties in a complementary fashion (Figure 4). Such 1D tapes are packed in a parallel fashion (see the Supporting Information, Tables S4 and S9 and Figures S3 and S8).

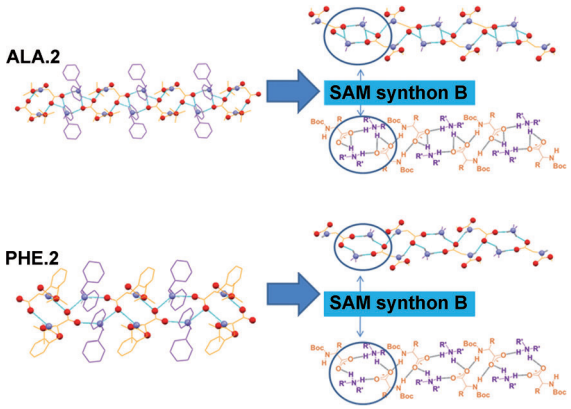

Figure 4. Left: 1D hydrogen-bonded tape in the crystal structures of **ALA.2** and **PHE.2**. Right: details of 1D hydrogen-bonded tape, wherein Boc-protected N–H takes part in hydrogen bonding; the existence of discrete **SAM** synthon B is marked; (the side chain of the amino acid and the ammonium cation are hidden for better clarity).

Thus, it is clear that despite the presence of a hydrogen-bond donor such as Boc-protected N–H in the amino acid moiety, all the salts displayed 1D HBNs; a typical 1D **SAM** synthon A is present in two cases (**LEU.1** and **PHE.1**), whereas Boc-protected N–H participates in hydrogen bonding in three cases (**LEU.2, ILE.2**, and **GLY.2**) resulting in a 1D tape with 1D **SAM** synthon A. 1D tape HBNs are also observed in two cases (**ALA.2** and **PHE.2**), wherein the discrete **SAM** synthon B is propagated through complementary dimeric N–H···O interactions involving the Boc-protected N–H and carboxylate O atoms. It may be important to note that in all the cases, the powder X-ray diffraction (PXRD) patterns (simulated from the single-crystal X-ray data and that of as-synthesized solids) are nearly superimposable, which indicates high crystalline phase purity of the salts except in **LEU.1** (see the Supporting Information, Figure S9).

A Cambridge structural database (CSD; version 1.13, Nov. 2010) search using a Boc-protected α-amino acid carboxylate fragment yielded only nine hits of which seven are organic salts of various amines; interestingly, the amine used in two of these seven salts (REFCODE: JAFMOS and SEZLOZ) is dicyclohexylamine, which is also used in the present study; both these structures display a 1D HBN. Although SEZLOZ (dicyclohexylammonium Boc-threoninate) showed a 1D tape involving synthon A, JAFMOS (dicyclohexylammonium Boc-β-methyl phenulalaninate) displayed a typical 1D **SAM** synthon A (see the Supporting Information, Figure S10).

Gelation studies: Since all these salts showed 1D HBN including the typical **SAM** synthon A that is implicated in gel formation (see above), we evaluated the gelation properties of the salts. The salts were scanned for gelation in 13 different organic solvents (see the Supporting Information, Table S10). Most of the salts turned out to be highly soluble in the solvents studied and produced well-shaped crystals. Many of the salts produced gelatinous precipitates. The salts

GLY.1, **GLY.2**, and **ALA.1** showed reasonable gelation abilities with a few solvents. **GLY.1** gelled only nitrobenzene, with a minimum gelator concentration (MGC) of 2.0 wt% and a gel melting temperature T_{gel} of 69°C. **GLY.2** gelled both nitrobenzene (MGC = 4.0 wt%, T_{gel} = 52°C) and methylsalicylate (MGC = 4.0 wt%, T_{gel} = 67°C). **ALA.1** gelled a much less polar solvent, *o*-xylene (MGC = 8 wt%, T_{gel} = 48°C).

Mouldablity, load-bearing and self-healing properties of GLY.1: A nitrobenzene gel (7 wt%) of **GLY.1** was found to be a free-standing gel, meaning that a piece of gel could be left as such without any confinement within a container (Figure 5A). It also had a remarkable load-bearing capacity, as demonstrated in Figure 5B, where we show that 13

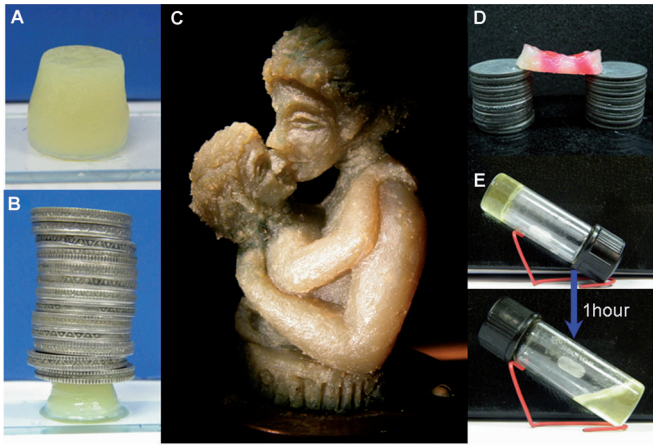

Figure 5. A) Free-standing gel (7.0 wt%, nitrobenzene) of **GLY.1**; B) the free-standing gel of **GLY.1** withstanding the pressure of 13 Indian 5 Rupee coins (≈117 g); C) a gel sculpture of "mother and child" made from a 7.0 wt% nitrobenzene gel of **GLY.1**; D) self-healing of five gel blocks of **GLY.1**; E) room temperature gel–sol transition of 5.0 wt% nitrobenzene gel of **GLY.2**.

Indian 5 Rupee coins (≈117 g) can be placed on a 0.17 in^2 area of a piece of free-standing gel (2 mL volume), which means that it can withstand a pressure of 1.4 psi (9.65 kPa). Such strength is remarkable for a non-polymeric supramolecular organogel and it encouraged us to attempt to create a sculpture using the gel. A solution of this gel was poured into a template of the sculpture, which depicts a mother and child. After cooling, the gel sculpture (Figure 5C) was taken out with care and it was found to be stable under ambient conditions for months (see the Supporting Information, Figure S11). The same gel also displayed self-healing behavior (Figure 5D). For this experiment, a block of a gel (3.0×0.8×0.6 cm) was cut into five pieces. Alternating pieces were dyed with Rhodamine B and the pieces were put together and allowed to self-heal. As shown by Figure 5D, the pieces of gel healed within a minute to form a single structure, and the whole structure is strong enough to hold its weight when placed on two columns separated by 2.0 cm. Since the HBN in the crystal structure of **GLY.1** is 1D and believed to be responsible for gel network formation, keeping two pieces of gel together for a minute appears to be good enough to reconstruct the HBN in the interface and thus leads to self-healing. In comparison to **GLY.1**, when the cation is changed to dibenzylammonium as in **GLY.2**, the corresponding gel was found to be unstable (Figure 5E). These results clearly emphasize the role of gel-network-solvent interactions, which are poorly understood. Changing the alicyclic cation to an aromatic cation in going from **GLY.1** to **GLY.2**, the gel-network-solvent interactions must not favor the formation of a strong gel with nitrobenzene.

Microscopy: We carried out both optical microscopy (OM) and scanning electron microscopy (SEM) of nitrobenzene gels of **GLY.1** and **GLY.2**. A highly entangled gel network comprised of thin fibrils is seen in the nitrobenzene gel of **GLY.1**, whereas micro-thin needle-shaped crystals could be observed in the corresponding gel of **GLY.2**. Similar morphological features are also seen in the SEM micrographs of the corresponding gels. The lack of a network on the microscale in the images of the **GLY.2** gel may explain its weaker mechanical properties compared with that of the **GLY.1** gel (Figure 6).

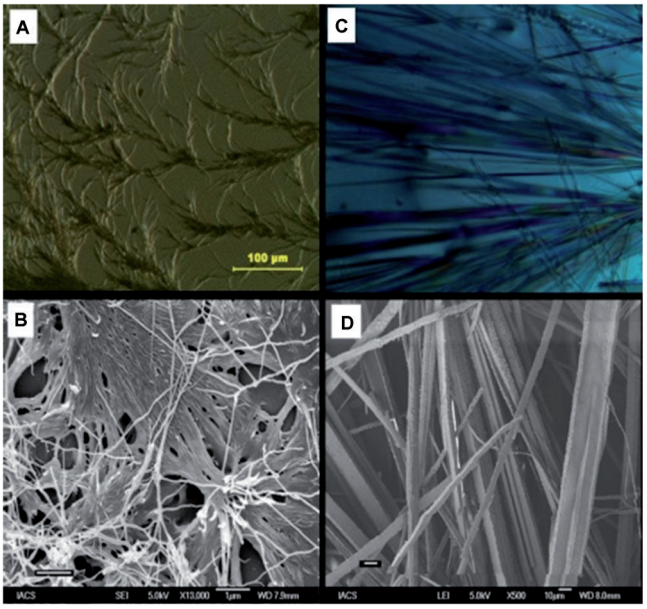

Figure 6. Nitrobenzene gel of A) OM of 2.0 wt% nitrobenzene gel of **GLY.1**; B) SEM of 1.0 wt% nitrobenzene gel of **GLY.1**; C) OM of 4.0 wt% nitrobenzene gel of **GLY.2**; D) SEM of 2.0 wt% nitrobenzene gel of **GLY.2**.

Rheology: A T_{gel} versus [gelator] plot of nitrobenzene gels derived from **GLY.1** and **GLY.2** displayed a steady increase in T_{gel} with the increase in [gelator]; this indicates that the gel networks are governed by noncovalent interactions such as hydrogen bonding; the greater strength of the **GLY.1** gel compared with the **GLY.2** gel is also clear from this plot (Figure 7). It is interesting to note that the PXRD of the ni-

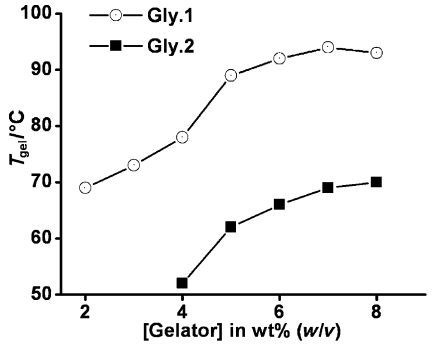

Figure 7. T_{gel} versus [gelator] plot of **GLY.1** and **GLY.2**.

trobenzene xerogel of **GLY.1** matched reasonably well with that of the experimental bulk solid and simulated pattern obtained from the single-crystal structure of **GLY.1** which means that the 1D HBN observed in the crystal structure of **GLY.1** is also present in the gel network of the xerogel (see the Supporting Information, Figure S9).

We conducted rheological experiments on a 7 wt% **GLY.1** gel in nitrobenzene. Figure 8a shows data from a dynamic frequency spectrum, which was conducted at a constant stress within the linear viscoelastic region of the sample. The data show that the elastic modulus G' exceeds the viscous modulus G'' over the entire range of frequencies ω. At high ω, G' approaches a plateau modulus ($G_p \approx 300$ kPa). Also, note that at high ω, the value of G' is much higher

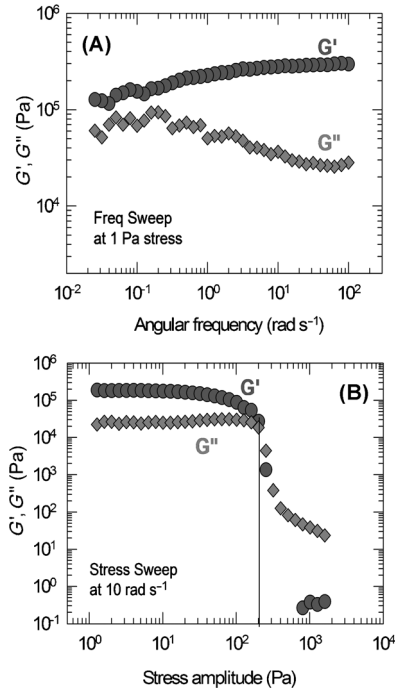

Figure 8. Dynamic rheological data on a 7 wt% **GLY.1** gel in nitrobenzene. A) Frequency sweep showing the elastic modulus G' and the viscous modulus G'' as functions of angular frequency ω. B) Stress sweep showing G' and G'' as functions of stress amplitude σ at constant $\omega = 10$ rad s^{-1}. A sharp decrease in G' and G'' occurs at a value of s marked by the vertical line, which is the yield stress σ_y of the sample.

than that of G'' (in turn, tan $\omega = G''/G' \approx 0.1$), which implies that the response is strongly elastic at short timescales. On the other hand, at low ω, G' and G'' become much closer and both moduli show a weak frequency dependence (in turn, tan $\omega = G''/G' \approx 0.6$ to 0.8). This means that at long timescales, the sample shows some viscous character and exhibits a very slow relaxation process. A similar shape of the frequency spectrum was observed at all concentrations of **GLY.1** tested. We surmise that the weak relaxation at long timescales is conducive to the self-healing character of this gel.

Figure 8b shows a dynamic stress sweep, which was conducted at a constant frequency of 10 rad s^{-1}. Here the moduli are plotted as functions of the stress amplitude σ and we see the typical behavior of a shear thinning or thixotropic material. The moduli are both relatively constant at low stress amplitudes, with G' being considerably higher than G'', consistent with the frequency data (Figure 8a) at this frequency. However, when the stress is increased beyond about 300 Pa, the moduli rapidly plummet and G' falls below G''. This type of response indicates the yielding of the sample at high deformations, that is, the disruption of bonds in the network. The stress at which the moduli begin to plummet can be termed the yield stress σ_y of the gel and its value here is about 200 Pa (this is marked by the vertical line on Figure 8b). This is a high value of the yield stress, and it reflects the free standing and load bearing nature of the sample.

Interestingly, this gel also shows rapid recovery from shearing (Figure 9). For this experiment, we sheared the sample at a high oscillatory stress of 500 Pa (beyond σ_y) for a period of 2 min and then switched to a low stress within the linear viscoelastic region. At high stress, the sample exhibited a viscous response ($G'' > G'$) with low values of G' ($\approx$10 Pa), which indicates a disruption of its network structure. When switched to low stress, the sample instantaneous-

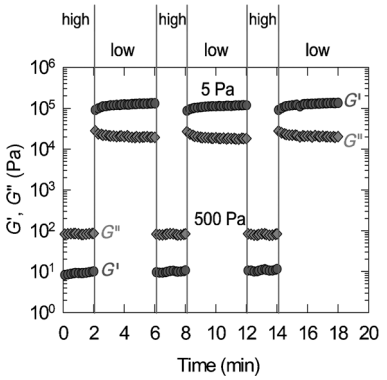

Figure 9. Cycling of a 7 wt% **GLY.1** gel in nitrobenzene between high and low extents of oscillatory shear. First, the sample is vigorously sheared for 2 min at an oscillatory stress amplitude of 500 Pa, which is well beyond its yield stress σ_y. For the next 4 min, the sample is switched to a low stress amplitude of 5 Pa, which is within its linear viscoelastic region. This cycle is then repeated twice more. The frequency is fixed at 10 rad s^{-1} for all these experiments. Note that the sample instantaneously recovers to its gel-like state as soon as the vigorous shear is switched off.

ly reverted to an elastic response ($G' > G''$) with high values of G' ($\approx$100 kPa), which indicated that the bonds in the network are quickly re-formed. The above cycle was repeated twice and the same behavior was observed. In summary, the noteworthy rheological properties of **GLY.1** gels are: 1) a high plateau modulus ($G_p \approx 300$ kPa); 2) a high yield stress ($\sigma_y \approx 200$ Pa); 3) a weak decay of G' and G'' at low ω indicating slow dissipative dynamics; and 4) quick recovery after disruptive shearing.

Conclusion

A supramolecular synthon approach led to the discovery of an organogel derived from an easily accessible organic salt (**GLY.1**); the nitrobenzene gel of **GLY.1** displayed remarkable moldable, load-bearing, and self-healing properties that are thus far confined to clay- and polymer-based gels with a few exceptions.[6] The strength of the **GLY.1** gel is so much so that a small piece of free standing gel (2.0 mL volume; 0.17 in^2 area) can withstand a pressure of 9.65 kPa and also allowed us to create a relatively large sculpture of "mother and child" that did not deform for months. These remarkable properties displayed by **GLY.1** and the inability of its dibenzylammonium counterpart (**GLY.2**) to display such properties were explained using microscopic and rheological data. The fact that such remarkable properties arising from an easily accessible (by salt formation) small molecule (the molecular weight of **GLY.1** is only 256.38) are due to noncovalent supramolecular interactions is quite intriguing. The results presented herein are expected to attract the attention of research groups interested in developing materials displaying such intriguing mechanical properties.[23]

Experimental Section

Materials and methods: All of the chemicals (Aldrich) and solvents (A.R. grade, commercially available, India) were used without any further purification. Petrol used in the gelation experiments was purchased from the local market. Microanalyses were performed on a Perkin–Elmer elemental analyzer 2400, Series II. FTIR spectra are recorded using Perkin–Elmer Spectrum GX. Powder X-ray patterns were recorded on an XPERT Philips diffractometer ($Cu_{K\alpha}$ radiation, $\lambda = 1.5418$ Å). Scanning electron microscopy (FTSEM) was performed on a JEOL; JSM-6700F. Single-crystal X-ray diffraction was done with a Bruker axs, SMART APEX II. Rheological experiments were performed on an AR2000 stress-controlled rheometer (TA Instruments). Samples were run on cone and plate geometries (20 mm diameter/2° cone angle or 40 mm diameter/4° cone angle). The plates were equipped with Peltier-based temperature control and all samples were studied at 25 ± 0.1 °C. A solvent trap was used to minimize evaporation of solvent.

Preparation of salts: Salts were prepared by mixing Boc-protected amino acids, namely glycine, alanine, valine, leucine, isoleucine, and phenylalanine with the corresponding dicyclohexylamine and dibenzylamine according to Scheme 2 in 1:1 molar ratio in methanolic medium. The resultant mixture was subjected to sonication for a few minutes to ensure the homogenous mixing of the two components. A white precipitate was obtained after complete removal of MeOH by rotary evaporator, which was subjected to various physico-chemical analyses and a gelation test.

Crystal structures: Data were collected using $Mo_{K\alpha}$ ($\lambda = 0.7107$ Å) radiation on a Bruker APEX II diffractometer equipped with a CCD area detector. Data collection, data reduction, structure solution/refinement were carried out using the software package of SMART APEX. All structures were solved by direct methods and refined in a routine manner. Non-hydrogen atoms were treated anisotropically. All the hydrogen atoms were geometrically fixed. CCDC-844914 (**GLY.1**), CCDC-811915 (**GLY.2**), CCDC-827781 (**ALA.2**), CCDC-811916 (**LEU.1**), CCDC-811917 (**LEU.2**), CCDC-811918 (**ILE.2**), CCDC-811919 (**PHE.1**) and CCDC-811920 (**PHE.2**) contain the supplementary crystallographic data for this paper. These data can be obtained free of charge from The Cambridge Crystallographic Data Centre via www.ccdc.cam.ac.uk/data_request/cif.

Acknowledgements

P.D. thanks the CSIR (New Delhi, India) for financial support. P.S. thanks the IACS for a research fellowship. H.Y.L. was partially funded by a grant from the Chemistry division of the National Science Foundation.

[1] Q. Wang, J. L. Mynar, M. Yoshida, E. Lee, M. Lee, K. Okuro, K. Kinbara, T. Aida, *Nature* **2010**, *463*, 339.
[2] V. Amendola, M. Meneghetti, *Nanoscale* **2009**, *1*, 74.
[3] G. Deng, C. Tang, F. Li, H. Jiang, Y. Chen, *Macromolecules* **2010**, *43*, 1191.
[4] S. Abdurrahmanoglu, V. Can, O. Okay, *Polymer* **2009**, *50*, 5449.
[5] D. C. Tuncaboylu, M. Sari, W. Oppermann, O. Okay, *Macromolecules* **2011**, *44*, 4997.
[6] A. Vidyasagar, K. Handore, K. M. Sureshan, *Angew. Chem.* **2011**, *123*, 8171; *Angew. Chem. Int. Ed.* **2011**, *50*, 8021.
[7] P. Dastidar, *Chem. Soc. Rev.* **2008**, *37*, 2699.
[8] R. G. Weiss, P. Terech, in *Molecular Gels: Materials with Self-Assembled Fibrillar Networks*, Springer, Dordrecht, **2006**.
[9] A. R. Hirst, B. Escuder, J. F. Miravet, D. K. Smith, *Angew. Chem.* **2008**, *120*, 8122; *Angew. Chem. Int. Ed.* **2008**, *47*, 8002.
[10] S. Datta, S. Bhattacharya, *Chem. Commun.* **2012**, *48*, 877.
[11] J. A. Foster, M.-O. M. Piepenbrock, G. O. Lloyd, N. Clarke, J. A. K. Howard, J. W. Steed, *Nat. Chem.* **2010**, *2*, 1037.
[12] Y. Gao, F. Zhao, Q. Wang, Y. Zhanga, B. Xu, *Chem. Soc. Rev.* **2010**, *39*, 3425.
[13] J. H. van Esch, *Langmuir* **2009**, *25*, 8392.
[14] G. R. Desiraju, *Angew. Chem.* **1995**, *107*, 2541; *Angew. Chem. Int. Ed. Engl.* **1995**, *34*, 2311.
[15] M. George, R. G. Weiss, *Acc. Chem. Res.* **2006**, *39*, 489.
[16] R. Luboradzki, O. Gronwald, M. Ikeda, S. Shinkaia, D. N. Reinhoudt, *Tetrahedron* **2000**, *56*, 9595.
[17] D. R. Trivedi, A. Ballabh, P. Dastidar, B. Ganguly, *Chem. Eur. J.* **2004**, *10*, 5311.
[18] D. R. Trivedi, P. Dastidar, *Cryst. Growth Des.* **2006**, *6*, 2114.
[19] D. R. Trivedi, P. Dastidar, *Cryst. Growth Des.* **2006**, *6*, 1022.
[20] D. R. Trivedi, A. Ballabh, P. Dastidar, *Chem. Mater.* **2003**, *15*, 3971.
[21] P. Dastidar, S. Okabe, K. Nakano, K. Iida, M. Miyata, N. Tohnai, M. Shibayama, *Chem. Mater.* **2005**, *17*, 741.
[22] D. R. Trivedi, A. Ballabh, P. Dastidar, *J. Mater. Chem.* **2005**, *15*, 2606.
[23] Note added in proof: While this paper was being reviewed, we came across two publications (T. Kishida, N. Fujita, K. Sada, S. Shinkai, *J. Am. Chem. Soc.* **2005**, *127*, 7298; S. Samai, K. Biradha, *Chem. Mater.* **2012**, *24*, 1165), wherein the mechanical strength of a gel was demonstrated by putting a number of coins on a small piece of gel as demonstrated in Figure 5b of this paper.

Received: March 22, 2012
Published online: May 24, 2012

CHEMISTRY
A EUROPEAN JOURNAL

Supporting Information

Gel Sculpture: Moldable, Load-Bearing and Self-Healing Non-Polymeric Supramolecular Gel Derived from a Simple Organic Salt

Pathik Sahoo,[a] Ravish Sankolli,[b] Hee-Young Lee,[c] Srinivasa R. Raghavan,[c] and Parthasarathi Dastidar*[a]

chem_201200986_sm_miscellaneous_information.pdf

SUPPORTING INFORMATION

Gel Sculpture: Moldable, Load-Bearing and Self-Healing Non-Polymeric Supramolecular Gel Derived from a Simple Organic Salt

Pathik Sahoo,[a] Ravish Sankolli,[b] Hee-Young Lee,[c] Srinivasa R. Raghavan[c] and Parthasarathi Dastidar*[a], parthod123@rediffmail.com; ocpd@iacs.res.in

[a]Department of Organic Chemistry, Indian Association for the Cultivation of Science (IACS), 2A & 2B Raja S. C. Mullick Road, Jadavpur, Kolkata – 700032, West Bengal, India
[b]Solid State and Structural Chemistry Unit, Indian Institute of Science, Bangalore – 560012, India
[c]Department of Chemical & Biomolecular Engineering, University of Maryland, College Park, MD 20742-2111, USA

Table of Content

Physico-chemical data…… S2 –S3

Table S1: Crystal data……. S4

Ortep Plot, Hydrogen bonding table (S2) and
Molecular parking diagram (Fig. S1) GLY.1……..S5

Ortep Plot, Hydrogen bonding table (S3) and
Molecular parking diagram (Fig. S2) GLY.2…… S6

Ortep Plot, Hydrogen bonding table (S4) and
Molecular parking diagram (Fig. S3) ALA.2……..S7

Ortep Plot, Hydrogen bonding table (S5) and
Molecular parking diagram (Fig. S4) LEU.1……..S8

Ortep Plot, Hydrogen bonding table (S6) and
Molecular parking diagram (Fig. S5) LEU.2……..S9

Ortep Plot, Hydrogen bonding table (S7) and
Molecular parking diagram (Fig. S6) ILE.2……S10

Ortep Plot, Hydrogen bonding table (S8) and
Molecular parking diagram (Fig. S7) PHE.1……..S11

Ortep Plot, Hydrogen bonding table (S9) and
Molecular parking diagram (Fig. S8) PHE.2……..S12

Gelation data table (S10)…….S13

PXRD of some gelator and nongelator salts (Fig. S9)……S14

SAM synthon observed (Fig. S10)……..S15

Gel Sculpture Preparation (Fig. S11)……..S16

Physico-chemical data for the salts

1. **DicyclohexylammoniumBoc-glycinate (GLY.1):** mp 171°C, Anal. Calc. for $C_{19}H_{36}N_2O_4$: C, 64.01; H,10.18; N, 7.86. Found: C, 64.19; H, 10.19; N, 7.95%. FT-IR (KBr): 3273, 2974, 2937, 2854, 2808, 2520, 1712, 1645, 1537, 1452, 1427, 1394, 1365, 1313, 1280, 1265, 1176, 1157, 1043, 952, 790, 709, 582cm^{-1}. ^{1}H NMR ($CDCl_3$) (300MHz) δ = 5.24 (brs, 1H), 3.69-3.68 (m, 2H, J = 3.3Hz), 3.01- 2.93 (m, 2H), 2.04-2.22 (m, 4H), 1.78 (m, 4H), 1.64 (brs, 3H), 1.47- 1.42 (m, 12H), 1.29- 1.18 (m, 6H).

2. **DibenzylammoniumBoc-L-glycinate (GLY.2):** mp 149- 151°C, Anal. Calc. for $C_{21}H_{28}N_2O_4$: C, 67.72; H, 7.58; N, 7.52. Found: C, 67.86; H, 7.72; N, 7.34%. FT-IR (KBr): 3338, 3064, 3035, 2974, 2935, 2754, 2603, 2482, 1706, 1629, 1571, 1515, 1452, 1419, 1400, 1367, 1315, 1278, 1244, 1172, 1151, 1211, 1047, 1024, 947, 920, 756, 702, 648, 592, 464cm^{-1}. ^{1}H NMR ($CDCl_3$) (300MHz) δ = 7.33- 7.30 (m, 10H), 5.11 (br, 1H), 3.83 (s, 4H), 3.67 (s, 1H), 1.44 (s, 9H).

3. **DicyclohexylammoniumBoc-L-alaninate (ALA.1):** mp 149°C, Anal. Calc. for $C_{20}H_{38}N_2O_4$: C, 64.83; H, 10.34; N,7.56. Found: C, 65.01; H, 10.51; N, 7.58 %. FT-IR (KBr): 3425, 2939, 2858, 2520, 1716, 1629, 1556, 1481, 1440, 1398, 1365, 1352, 1280, 1257, 1163, 1053, 1028, 848, 773, 630, 493, 466, 449 cm^{-1}. ^{1}H NMR ($CDCl_3$) (300MHz) δ = 5.408 (br, 1H), 4.037 (m, 1H), 3.030- 2.954 (m, 2H), 2.075- 2.037 (m, 4H), 1.966 (m, 4H,), 1.651 (brs, 2H), 1.429- 1.356 (m, 16H), 1.21(m, 6H).

4. **DibenzylammoniumBoc-L-alaninate (ALA.2):** mp 110°C, Anal. Calc. for $C_{22}H_{30}N_2O_4$: C, 68.37; H, 7.82; N,7.25. Found: C,68.23; H, 7.89; N, 7.12%. FT-IR (KBr): 3259, 3003, 2974, 2935, 2813, 2667, 1708, 1612, 1531, 1454, 1400, 1365, 1319, 1271, 1249, 1174, 1022, 999, 758, 740, 702, cm^{-1}. ^{1}H NMR ($CDCl_3$) (300MHz) δ = 9.017(br, 2H), 7.371-7.289 (m, 10H), 5.328- 5.311 (br, 1H), 4.065- 4.028 (m, 1H), 3.833 (s, 4H), 1.450 (s, 9H), 1.308 (d, J = 7.20Hz, 3H).

5. **DicyclohexylammoniumBoc-L-valinate (VAL.1):** mp 142 - 144°C, Anal. Calc. for $C_{22}H_{42}N_2O_4$: C, 66.29; H, 10.62; N,7.03. Found: C, 66.45; H, 10.83; N, 6.93%. FT-IR (KBr): 3435, 2941, 2860, 1716, 1629, 1554, 1483, 1392, 1365, 1313, 1247, 1164, 1085, 1035, 1016, 867, 763, 669, 486 cm^{-1}. ^{1}H NMR ($CDCl_3$) (300MHz) δ = 5.287 (d, J = 8.10Hz, 1H), 4.014- 3.974 (m, 1H), 3.058- 2.967 (m, 2H), 2.184- 2.065 (m, 4H), 1.838-1.511 (m, 11H), 1.452 (s, 9H), 1.319- 1.174 (m, 6H), 0.980 (d, J = 6.84,3H), 0.900 (d, J = 6.84, 3H).

6. **DibenzylammoniumBoc-L-valinate (VAL.2):** mp 96- 98°C, Anal. Calc. for $C_{24}H_{34}N_2O_4$: C, 69.54; H,8.27; N,6.76. Found: C, 69.49; H, 8.19; N, 6.68%. FT-IR (KBr): 3319, 2966, 2914, 1706, 1651, 1508, 1456, 1442, 1398, 1367, 1340, 1305, 1251, 1174, 1012, 968, 758, 740, 702, 578 cm^{-1}. ^{1}H NMR ($CDCl_3$) (300MHz) δ = 7.388- 7.317 (m, 10H), 7.041 (br, 2H), 5.169 (d, 1H, J = 8.46Hz), 4.067- 4.026 (m, 1H), 3.872 (s, 1H), 2.147- 2.087 (m, 1H), 1.446 (s, 9H), 0.935 (d, J = 0.935, 3H), 0.851 (d, J = 6.81, 3H).

7. **DicyclohexylammoniumBoc-L-leucinate (LEU.1):** mp 117 - 120°C, Anal. Calc. for $C_{22}H_{44}N_2O_4$: C, 66.95; H, 10.75; N, 6.79. Found: C, 66.96; H, 10.37; N, 6.80 %. FT-IR (KBr): 3433, 3404, 3296, 2935, 2858, 2470, 1712, 1633, 1554, 1481, 1467, 1452, 1402, 1363, 1269, 1249, 1174, 1118, 1051, 1012, 875, 846, 785, 752, 657, 592, 559, 488, 447 cm^{-1}. ^{1}H NMR (D_2O) (300MHz) δ = 3.80 (t, J = 6.67Hz, 1H), 3.15- 3.12 (m, 2H), 1.94

(m, 4H), 1.71 (m, 4H), 1.592- 1.551 (m, 3H), 1.436- 1.391 (m, 2H), 1.327 (s, 9H), 1.209- 1.174 (m, 7H), 1.142- 1.035 (m, 3H), 0.829- 0.790 (m, 6H)

8. **DibenzylammoniumBoc-l-leuciinate (LEU.2):** mp 134°C, Anal. Calc. for $C_{25}H_{36}N_2O_4$: C, 70.06; H,8.47; N, 6.54. Found: C,70.29; H,8.46; N, 6.36 %. FT-IR (KBr): 3340, 2968, 2947, 1706, 1647, 1564, 1504, 1456, 1396, 1361, 1247, 1170, 1024, 929, 850, 758, 698, 617, 578 cm^{-1}. ^1H NMR ($CDCl_3$) (300MHz) δ = 7.420- 7.316(m, 10H), 5.124- 5.101 (br, 1H), 4.165 – 4.142 (m, 1H), 3.881 (s, 4H), 1.773 – 1.587 (M, 2H), 1.461 (s, 10H), 0.964 – 0.930 (m, 6H)

9. **DicyclohexylammoniumBoc-l-isoleucinate (ILE.1):** mp 129 - 131°C, Anal. Calc. for $C_{22}H_{44}N_2O_4$: C, 66.95; H, 10.75; N, 6.79. Found: C, 67.01; H, 10.74; N, 6.83 %. FT-IR (KBr): 4319, 2937, 2862, 2474, 2360, 1712, 1629, 1564, 1462, 1398, 1319, 1247, 1174, 1051, 1020, 868, 781, 657, 617, 596, 555, 489, 468 cm^{-1}. ^1H NMR ($CDCl_3$) (300MHz) δ = 5.330 (d, J = 7.65, 1H), 3.962- 3.938 (m, 1H), 2.996- 2.921 (m, 2H), 2.032- 1.996 (m, 4H), 1.811- 1.778 (m, 5H), 1.655 (m, 2H), 1.428 (m, 13H), 1.250- 1.209 (m, 7H), 0.941- 0.869 (m, 6H).

10. **DibenzylammoniumBoc-l-Isoleucinate (ILE.2):** mp 96°C, Anal. Calc. for $C_{25}H_{36}N_2O_4$: C, 70.06; H,8.47; N, 6.54. Found: C,70.14; H,8.39; N, 6.39 %. FT-IR (KBr): 3327, 2968, 2933, 1706, 1649, 1506, 1454, 1398, 1367, 1247, 1172, 1043, 1012, 802, 700, 590 cm^{-1}. ^1H NMR ($CDCl_3$) (300MHz) δ = 7.394- 7.290 (m, 10H), 5.218 (d, J = 8.40Hz, 1H), 4.086- 4.043 (m, 1H), 3.846 (s, 4H), 1.82 (br, 1H), 1.448 (s, 9H), 1.150- 1.074 (m, 1H), 0.905- 0.862 (6H).

11. **DicyclohexylammoniumBoc-l-phenylalaninate (PHE.1):** mp 228°C, Anal. Calc. for $C_{26}H_{42}N_2O_4$: C, 69.92; H, 9.48; N, 6.27. Found: C, 69.99; H, 9.50; N, 6.17 %. FT-IR (KBr): 3425, 3030, 2933, 2860, 2521, 2366, 1708, 1624, 1570, 1485, 1467, 1398, 1363, 1307, 1242, 1163, 1055, 1030, 989, 869, 823, 738, 700, 636, 559, 491, 461, 447 cm^{-1}. ^1H NMR ($CDCl_3$) (300MHz) δ = 7.245-7.160 (m, 5H), 5.175 (d, 1H, J = 7.50Hz), 4.404 (d, 1H, J = 6.00Hz), 3.219-2.952 (m, 4H), 2.076-1.189 (m, 29H).

12. **DibenzylammoniumBoc-l-phenylalaninate (PHE.2):** mp 130°C, Anal. Calc. for $C_{28}H_{34}N_2O_4$: C, 72.70; H,7.41; N, 6.06. Found: C,72.83; H, 7.16; N, 6.1 9 %. FT-IR (KBr): 3263, 3001, 2976, 1710, 1625, 1527, 1452, 1398, 1363, 1272, 1172, 1016, 790, 756, 700, 499 cm^{-1}. ^1H NMR ($CDCl_3$) (300MHz) δ = x.x (br, N-H), 7.377-7.310 (m, 10H), 7.204- 7.143 (m, 5H), 5.144 (m, 1H), 4.350 (m, 1H), 3.780- 3.763 (m, 4H), 3.196- 3.136 (m,1H), 3.030- 2.999 (m, 1H), 1.424 (s, 9H)).

Table S1 | Crystal data.

Crystal parameters	GLY.1	GLY.2	ALA.2	LEU.1	LEU.2	ILE.2	PHE.1	PHE.1
CCDC No	844914	811915	827781	811916	811917	811918	811919	811920
Empirical formula	$C_{19}H_{36}N_2O_4$	$C_{21}H_{28}N_2O_4$	$C_{22}H_{30}N_2O_4$	$C_{23}H_{44}N_2O_4$	$C_{25}H_{36}N_2O_4$	$C_{25}H_{36}N_2O_4$	$C_{26}H_{42}N_2O_4$	$C_{28}H_{34}N_2O_4$
Formula weight	356.50	372.45	386.48	412.60	428.56	428.56	446.62	462.57
Crystal size/mm	0.93 X 0.79 X 0.45	0.32 X 0.24 X 0.16	0.29 X 0.29 X 0.28	0.26 X 0.16 X 0.10	0.22 X 0.14 X 0.08	0.21 X 0.18 X 0.17	0.22 X 0.19 X 0.16	0.22 X 0.17 X 0.12
Crystal system	Triclinic	Monoclinic	Triclinic	Orthorhombic	Monoclinic	Monoclinic	Orthorhombic	Orthorhombic
Space group	P-1	$P2_1/n$	P1	$P2_12_12_1$	$P2_1$	$P2_1$	$P2_12_12_1$	$P2_12_12_1$
a /Å	5.8278(4)	9.2810(18)	10.326(4)	9.622(5)	5.948(5)	6.014(5)	9.337(6)	10.3172(9)
b/Å	12.2093(8)	24.260(5)	10.326(4)	16.222(5)	21.374(5)	17.441(5)	16.194(10)	22.396(2)
c /Å	15.7358(10)	9.6110(18)	12.605(5)	16.602(5)	9.803(5)	11.611(5)	17.005(10)	23.051(2)
$\alpha/^0$	108.816(3)	90.00	75.833(6)	90.000(5)	90.000(5)	90.000(5)	90.00	90.00
$\beta/^0$	91.192(3)	108.854(3)	70.249(6)	90.000(5)	100.069(5)	99.330(5)	90.00	90.00
$\gamma/^0$	96.468(3)	90.00	61.223(6)	90.000(5)	90.000(5)	90.000(5)	90.00	90.00
Volume/$Å^3$	1051.13(12)	2047.9(7)	1103.2(7)	2591.4(17)	1227.1(12)	1201.8(12)	2571(3)	5326.4(8)
Z	2	4	2	4	2	2	4	8
F(000)	392	800	416	912	464	464	976	1984
μ MoKα /mm^{-1}	0.078	0.084	0.080	0.071	0.078	0.080	0.077	0.077
Temperature/K	293(2)	298(2)	293(2)	298(2)	298(2)	298(2)	298(2)	298(2)
R_{int}	0.0270	0.0620	0.0425	0.1045	0.0675	0.0442	0.0609	0.0355
Range of h, k, l	-7/7, -15/15, -19/19	-10/10, -26/27, -10/10	-12/12, -12/12, -14/14	-11/11, -20/20, -20/20	-7/7, -26/26, -12/12	-7 /7, -21/21, -14/14	-10 /10, -17/17, -18/18	-12 /12, -28/28, -28/28
θmin/max/°	1.37/ 26.50	1.68/23.28	1.73/24.71	3.24/26.00	3.48/ 26.00	3.43/26.49	1.74 /23.18	1.27/ 26.56
Reflections collected/unique/ observed [I>2σ(I)]	11450/ 4351/ 3009	16646 /2938/2215	10199/3751/2388	20591/ 2874/ 1220	12640/ 2478 / 1816	13133 /2580/ 1943	14629 /2063 /1910	57200/ 6128 / 4941
Data/restraints/ parameters	4351/0/229	2938 /0/248	3751/3/513	2874 /0/267	2478/1/285	2580/1/285	2063/0/292	6128/0/619
Goodness of fit on F^2	1.036	0.821	1.123	0.816	0.948	0.933	1.007	1.025
Final R indices [I>2σ(I)]	R_1 = 0.0446 wR_2 = 0.1201	R_1 = 0.0387 wR_2 = 0.1081	R_1 = 0.0893 wR_2 = 0.2001	R_1 = 0.0451 wR_2 = 0.0820	R_1 = 0.0461 wR_2 = 0.1043	R_1 = 0.0388 wR_2 = 0.0752	R_1 = 0.0336 wR_2 = 0.0797	0.0386 0.0916
R indices (all data)	R_1 = 0.0683 wR_2 = 0.1367	R_1 = 0.0580 wR_2 = 0.1262	R_1 = 0.1348 wR_2 = 0.2256	R_1 = 0.1440 wR_2 = 0.0993	R_1 = 0.0650 wR_2 = 0.1115	R_1 = 0.0578 wR_2 = 0.0801	R_1 = 0.0370 wR_2 = 0.0817	0.0534 0.1028

Molecular Plots and Hydrogen Bonding Parameters for the compounds

Ortep Plot (50% probability) of DicyclohexylammoniumBoc-glycinate (GLY.1)

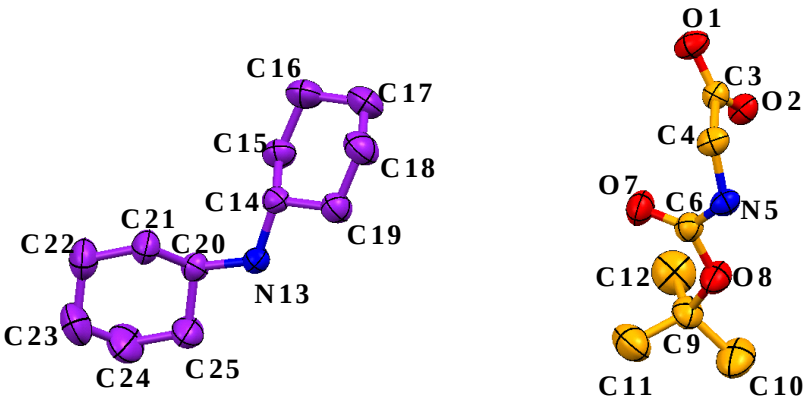

Table S2 | Hydrogen bonding parameters of GLY.1

D—H···*A*	*D*—H	H···*A*	*D*···*A*	*D*—H···*A*
N5—H5···O2^{i}	0.86	2.13	2.9289 (16)	154
N13—H13A ···O2^{ii}	0.90	1.80	2.6998 (15)	174
N13—H13B ···O1^{iii}	0.90	1.81	2.7081 (16)	172
Symmetry codes: (i) −*x*+2, −*y*+2, −*z*; (ii) *x*, *y*−1, *z*; (iii) *x*−1, *y*−1, *z*.				

Figure S1 | Molecular Packing of GLY.1

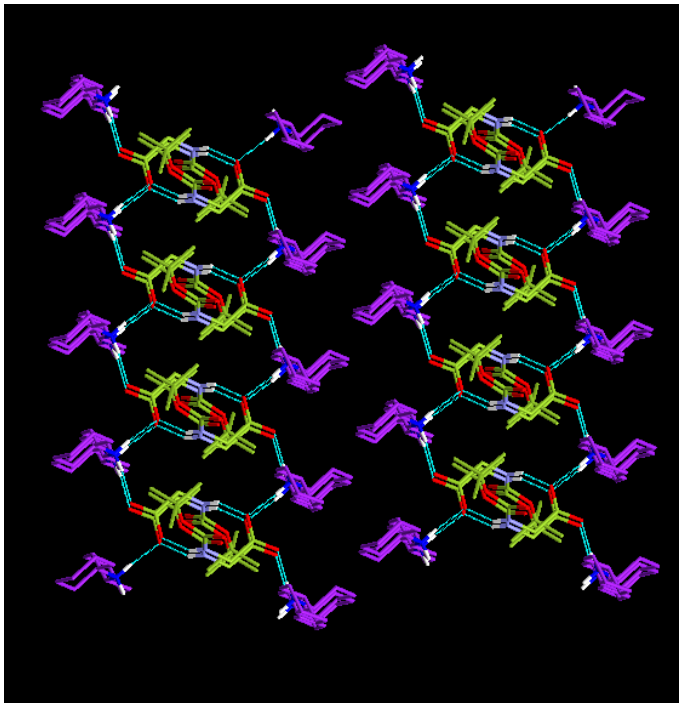

Ortep Plot (50% probability) of DibenzylammoniumBoc-L-glycinate (GLY.2)

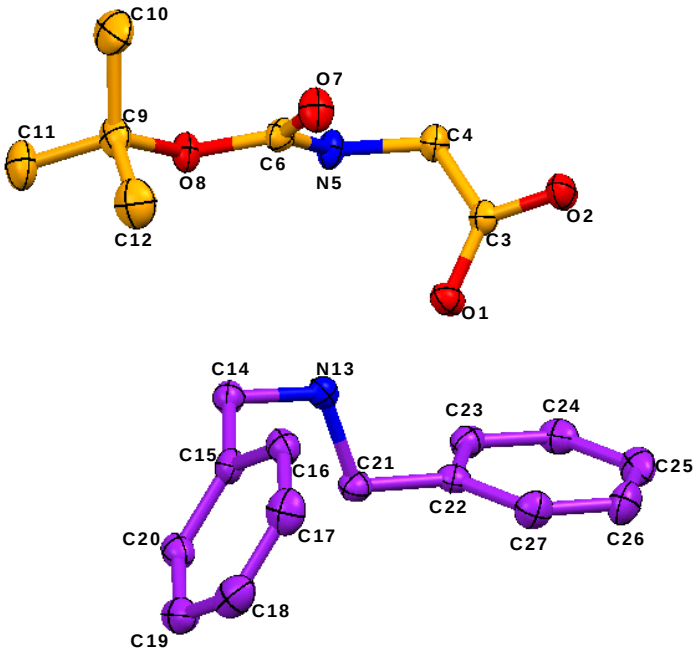

Table S3 | Hydrogen bonding parameters of GLY.2

D—H···*A*	*D*—H	H···*A*	*D*···*A*	*D*—H···*A*
N5—H5···O2^{i}	0.86	2.08	2.853 (2)	149.5
N13—H13A···O2^{i}	0.90	1.81	2.692 (2)	165.2
N13—H13A···O1^{i}	0.90	2.57	3.158 (2)	124.0
N13—H13B···O1	0.90	1.85	2.729 (2)	165.7
Symmetry codes: (i) x+1/2, -y+1/2, z+1/2.				

Figure S2 | Molecular Packing of GLY.2

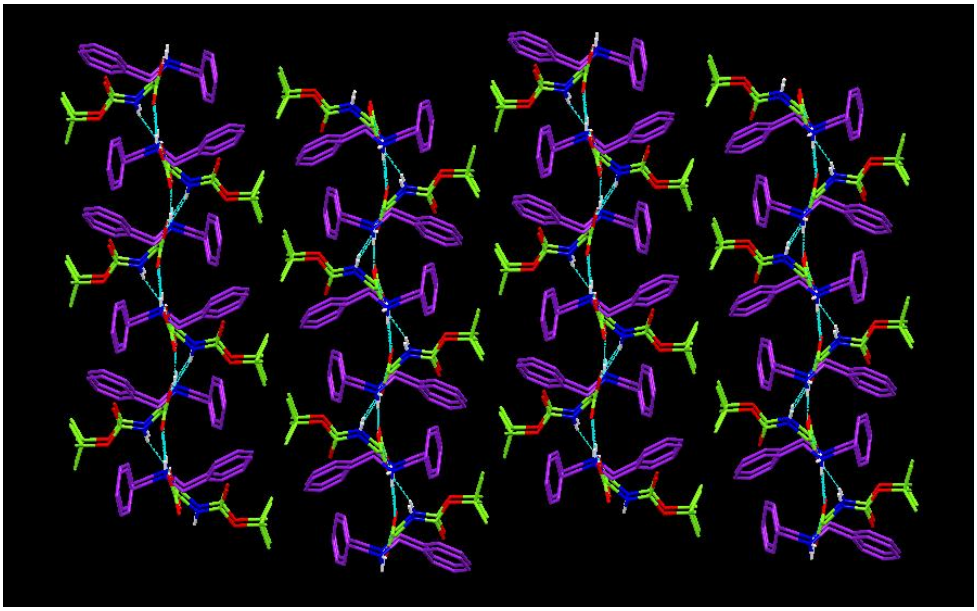

Ortep Plot (50% probability) of DibenzylammoniumBoc-L-alaninate (ALA.2)

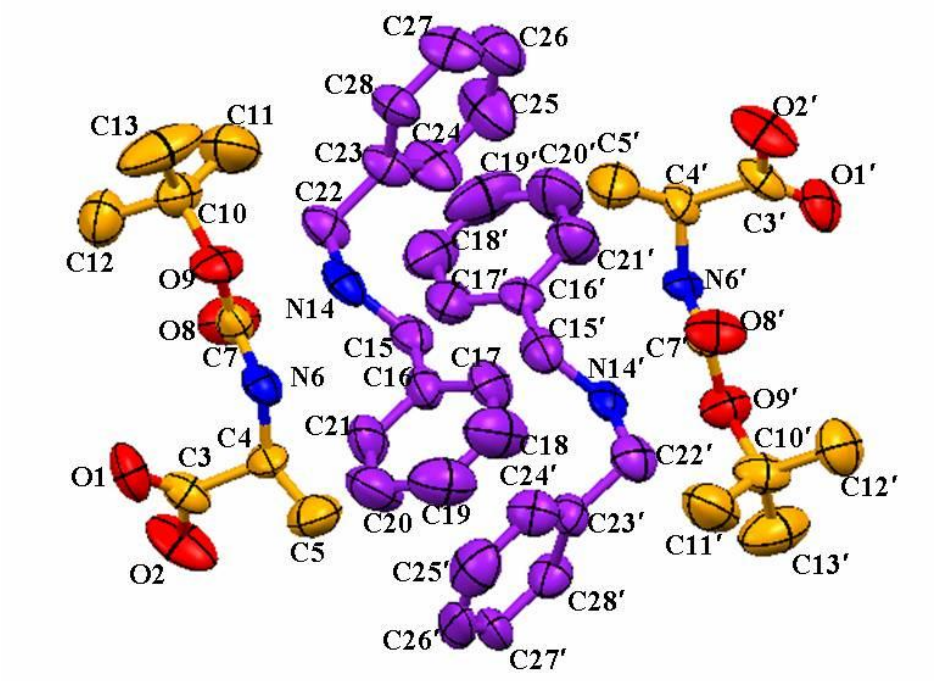

Table S4 | Hydrogen bonding parameters of ALA.2

D—H···*A*	*D*—H	H···*A*	*D*···*A*	*D*—H···*A*
N14′—H14*D*···O2′^{i}	0.90	1.80	2.660(9)	160
N14′—H14*C*···O1^{ii}	0.90	2.33	2.901(9)	131
N14′—H14*C*···O2^{ii}	0.90	2.03	2.854(11)	152
N6′—H6′···O1^{ii}	0.86	2.16	2.850(10)	137
N14—H14*B*···O1′^{iii}	0.90	2.16	2.859(9)	134
N14—H14*B*···O2′^{iii}	0.90	2.09	2.899(11)	150
N14—H14*A*···O2^{iv}	0.90	1.80	2.685(9)	166
N6—H6···O1′^{iii}	0.86	2.17	2.906(9)	143
Symmetry codes: (i) *x*, *y*+1, *z*; (ii)_ *x*+1, *y*−1, *z*; (iii) *x*−1, *y*+1, *z*; (iv) *x*, *y*−1, *z*				

Figure S3 | Molecular Packing of ALA.2

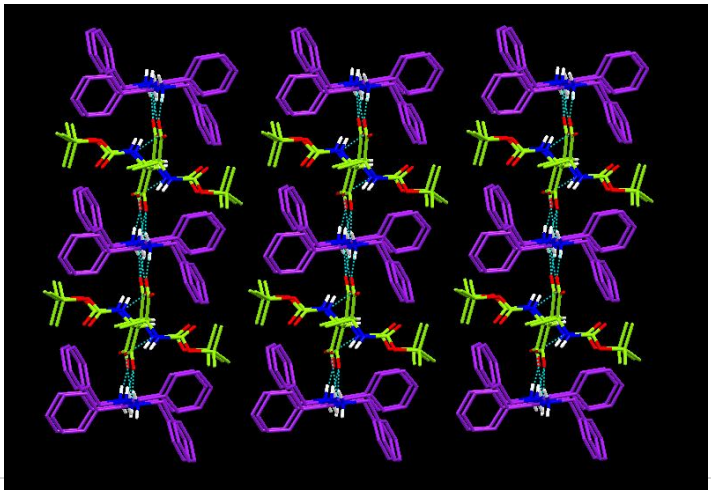

Ortep Plot (50% probability) of DicyclohexylammoniumBoc-L-leucinate (LEU.1)

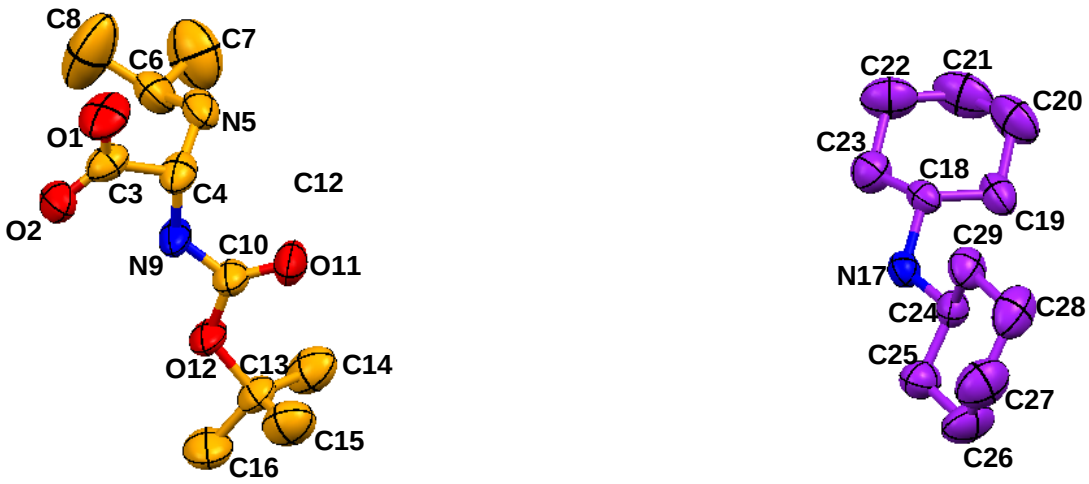

Table S5 | Hydrogen bonding parameters of LEU.1

D—H···*A*	*D*—H	H···*A*	*D*···*A*	*D*—H···*A*
N17—H17A···O1^{i}	0.90	1.86	2.743 (4)	167.4
N17—H17B···O2^{ii}	0.90	1.81	2.713 (4)	177.2
Symmetry codes: (i) *x*, *y*−1, *z*; (ii) *x*−1/2, −*y*+3/2, −*z*+1.				

Figure S4 | Molecular Packing of LEU.1

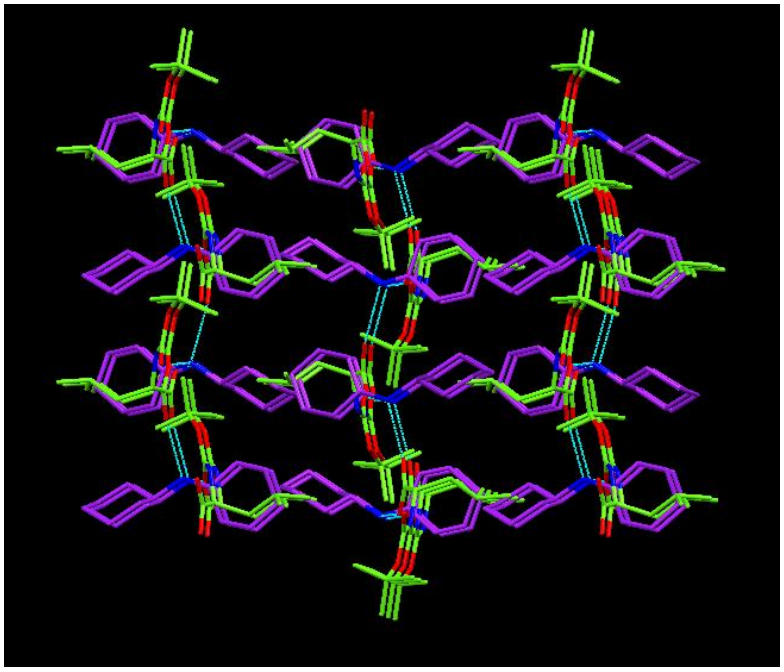

Ortep Plot (50% probability) of DibenzylammoniumBoc-L-leuciinate (LEU.2)

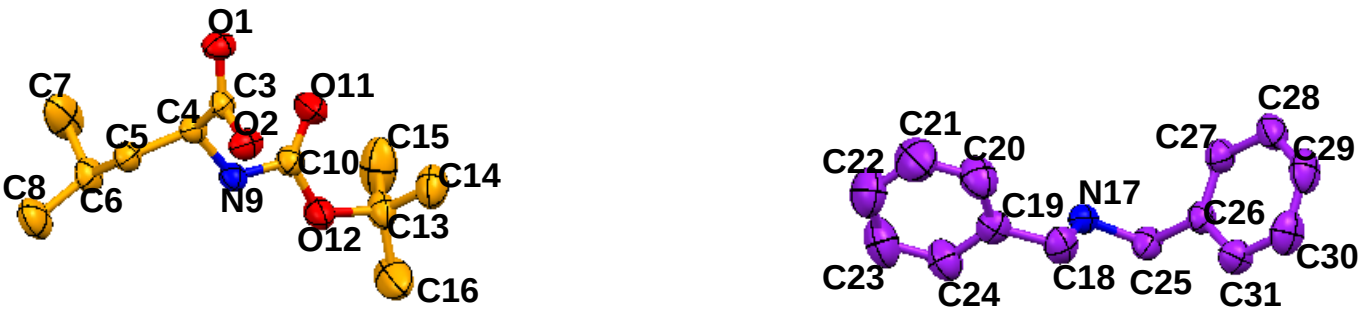

Table S6 | Hydrogen bonding parameters of LEU.2

LEU.2				
D—H···*A*	*D*—H	H···*A*	*D*···*A*	*D*—H···*A*
N9—H9···O1^{i}	0.86	2.24	3.085 (4)	166.6
N17—H17A···O2^{ii}	0.90	1.90	2.797 (4)	175.3
N17—H17B···O1^{iii}	0.90	1.80	2.678 (3)	165.6
D—H···*A*	*D*—H	H···*A*	*D*···*A*	*D*—H···*A*
Symmetry codes: (i) *x*−1, *y*, *z*; (ii) *x*, *y*+1, *z*; (iii) *x*−1, *y*+1, *z*.				

Figure S5 | Molecular Packing of LEU.2

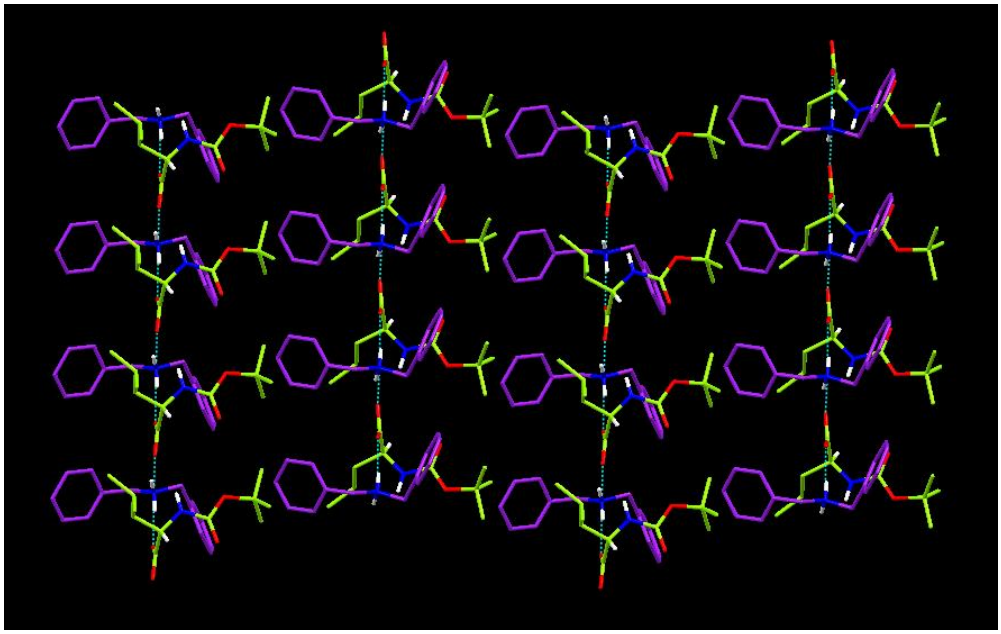

Ortep Plot (50% probability) of DibenzylammoniumBoc-L-isoleucinate (ILE.2)

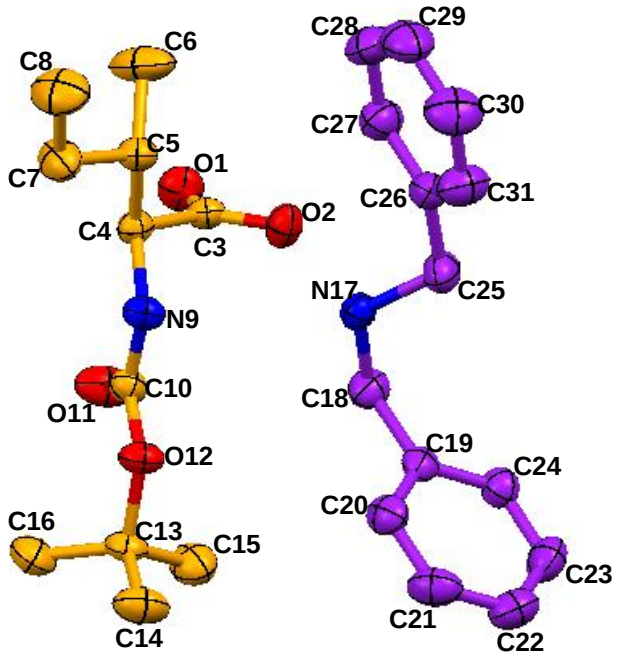

Table S7 | Hydrogen bonding parameters OF ILE.2

D—H···*A*	*D*—H	H···*A*	*D*···*A*	*D*—H···*A*
N9—H9···O1^{i}	0.86	2.23	3.058(3)	160.8
N17—H17A···O2	0.90	1.89	2.698(3)	147.9
N17—H17B···O1^{i}	0.90	1.82	2.688(3)	161.1
Symmetry codes: (i) *x*+1, *y*, *z*.				

Figure S6 | Molecular Packing OF ILE.2

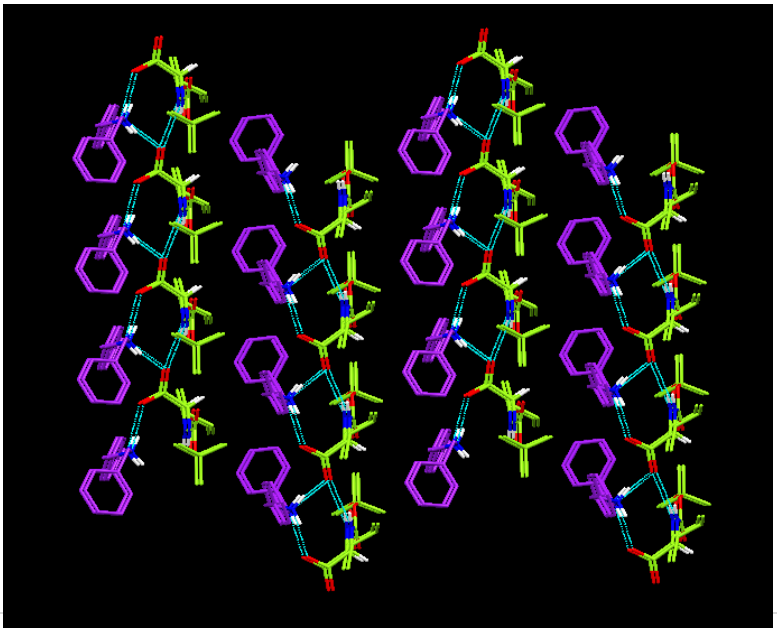

Ortep Plot (50% probability) of DicyclohexylammoniumBoc-L-phenylalaninate (PHE.1)

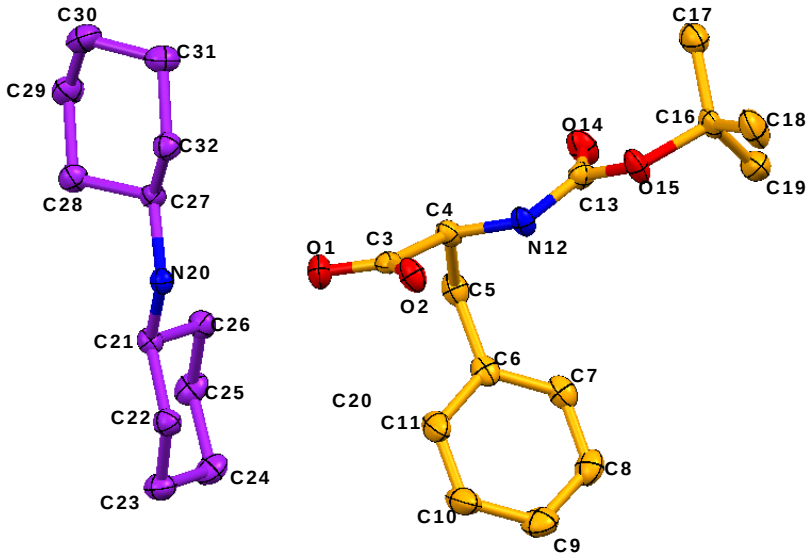

Table S8 | Hydrogen bonding parameters of PHE.1

D—H···*A*	*D*—H	H···*A*	*D*···*A*	*D*—H···*A*
N20—H20B···O2^{i}	0.90	1.80	2.700 (3)	173.1
N20—H20A···O1	0.90	1.89	2.748 (3)	157.6
Symmetry codes: (i) *x*+1/2, −*y*+1/2, −*z*.				

Figure S7 | Molecular Packing of PHE.1

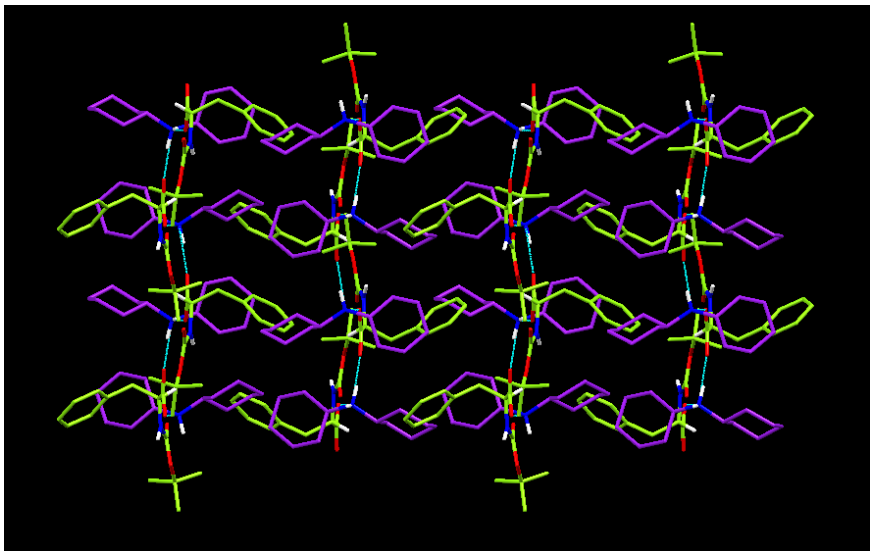

Ortep Plot (50% probability) of DibenzylammoniumBoc-L-phenylalaninate (PHE.2)

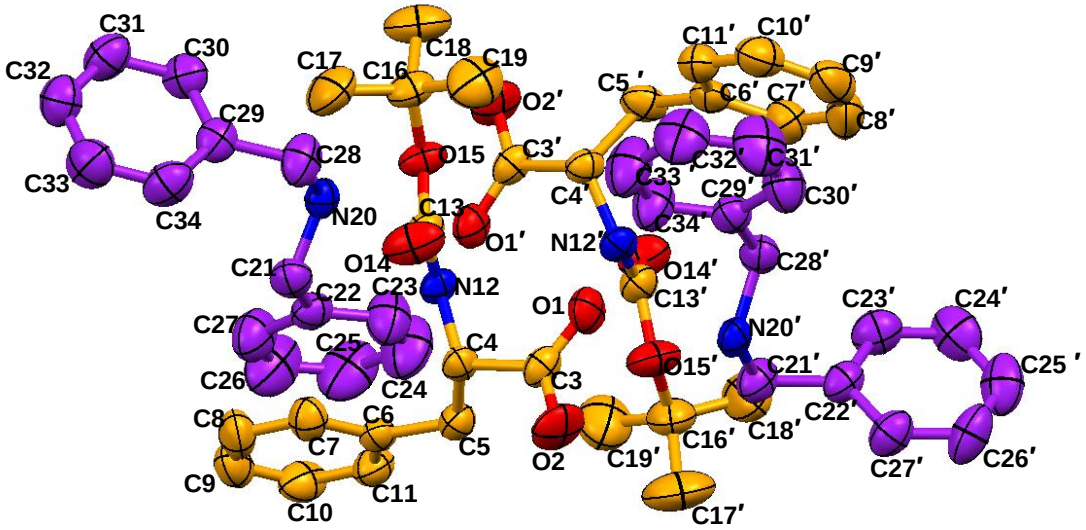

Table S9 | Hydrogen bonding parameters of PHE.1

D—H···*A*	*D*—H	H···*A*	*D*···*A*	*D*—H···*A*
N20'—H20D···O2'^{i}	0.90	1.82	2.712 (2)	169.8
N20'—H20C···O1	0.90	1.96	2.723 (2)	141.1
N20—H20B···O1'	0.90	1.90	2.706 (2)	147.9
N20—H20A···O2^{ii}	0.90	1.81	2.679 (2)	162.7
N12'—H12'···O1	0.86	2.11	2.902 (3)	153.3
N12—H12···O1'	0.86	2.19	2.995 (2)	156.0
Symmetry codes: (i) *x*−1, *y*, *z*; (ii) *x*+1, *y*, *z*.				

Figure S8 | Molecular Packing of PHE.1

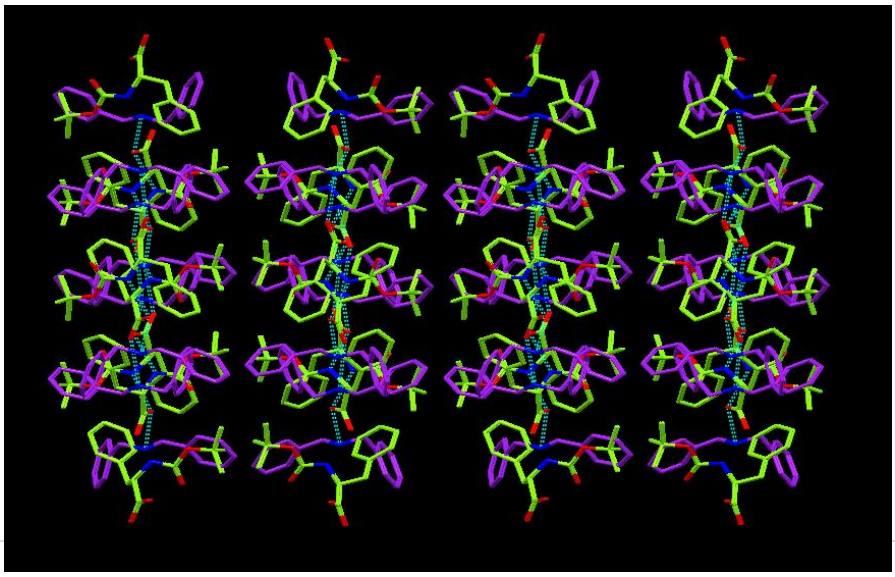

Table S10 | Gelation data

Salt	DMSO	DMF	Methyl salicylate	$PhNO_2$	PhCl	1,2-dichloro benzene	Ph-Me	o-Xylene	m-Xylene	p-Xylene	H_2O	MeOH	Petrol
GLY.1	WG	WG	S	2(69^0C)	GP	S	WG	WG	WG	WG	S	S	WG
GLY.2	S	S	4(67^0C)	4(67^0C)	US	US	WG	WG	WG	WG	BC	S	PPT
ALA.1	GP	WG	S	S	S	S	S	8(48^0C)	WG	S	S	S	S
ALA.2	S	HS	S	S	S	S	S	S	S	S	S	S	CP
VAL.1	GP	S	S	S	S	S	S	S	S	S	NC	S	NC
VAL.2	S	S	S	S	S	S	S	S	S	S	GP	S	S
LEU.1	S	S	S	S	S	S	S	S	S	S	S	S	S
LEU.2	S	S	US	S	S	US	BC	BC	BC	BC	NC	S	BC
ILE.1	S	S	S	S	S	S	S	S	S	S	S	S	S
ILE.2	S	S	S	S	S	S	S	S	S	S	S	S	BC
PHE.1	S	S	S	S	P	P	CP	CP	CP	CP	CP	CP	CP
PHE.2	S	S	P	S	S	S	P	P	P	P	P	P	P

[a]Numerical values indicate minimum gelator concentration in wt% (W/V); numerical values within parenthesis are gel-sol dissociation temperature in °C; WG- weak gel; GP- gel precipitate; US- upper layer sealed with a thin layer of gel-like material; P- precipitate; CP- crystalline precipitate; NC- Needle crystal; S- solution; BC - block shaped crystal.

Figure S9 | PXRD of some gelator and nongelator salts at various conditions

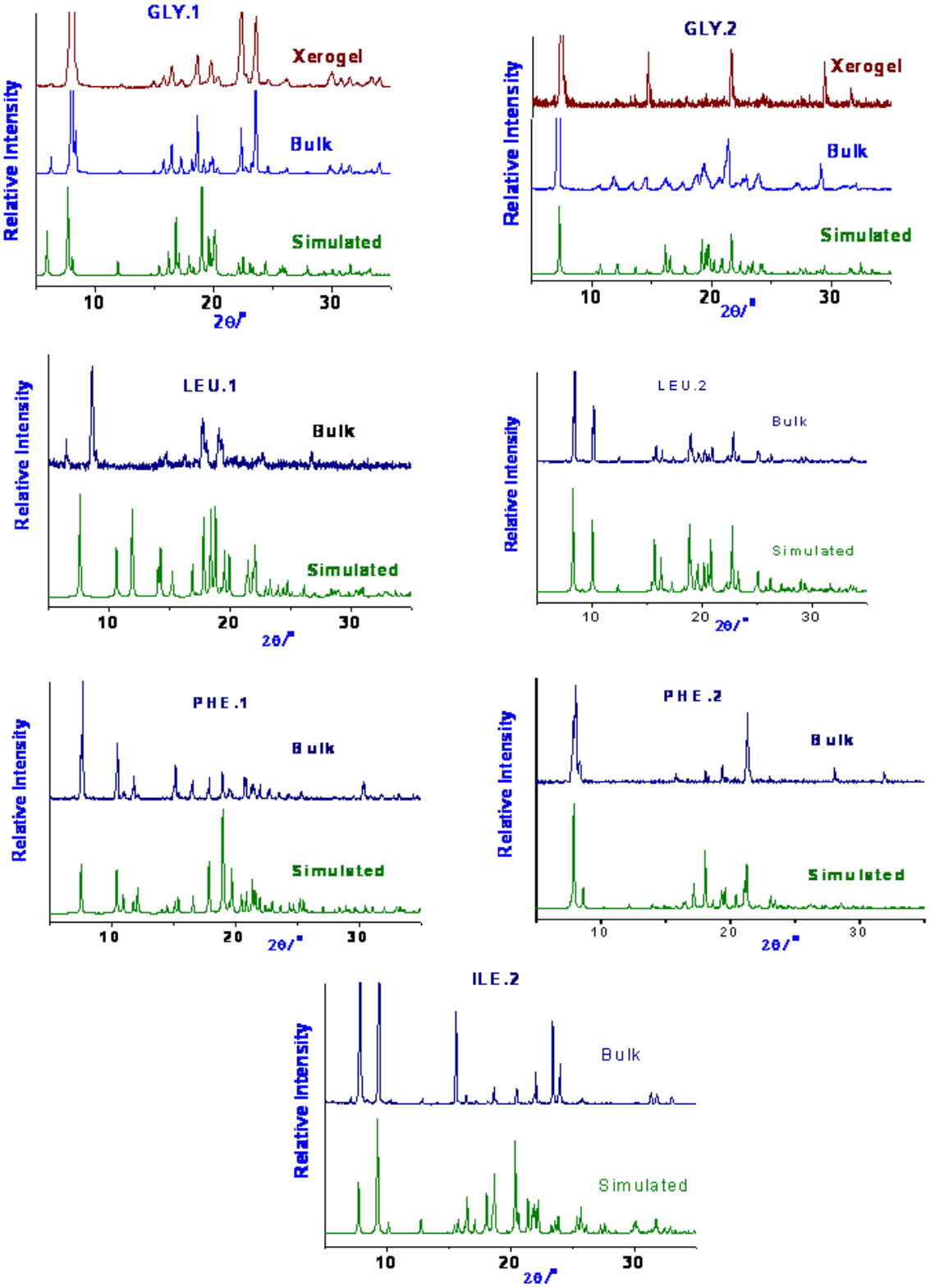

Figure S10 | SAM synthon observed in the crystal structures of various SAM salts deposited in CSD.

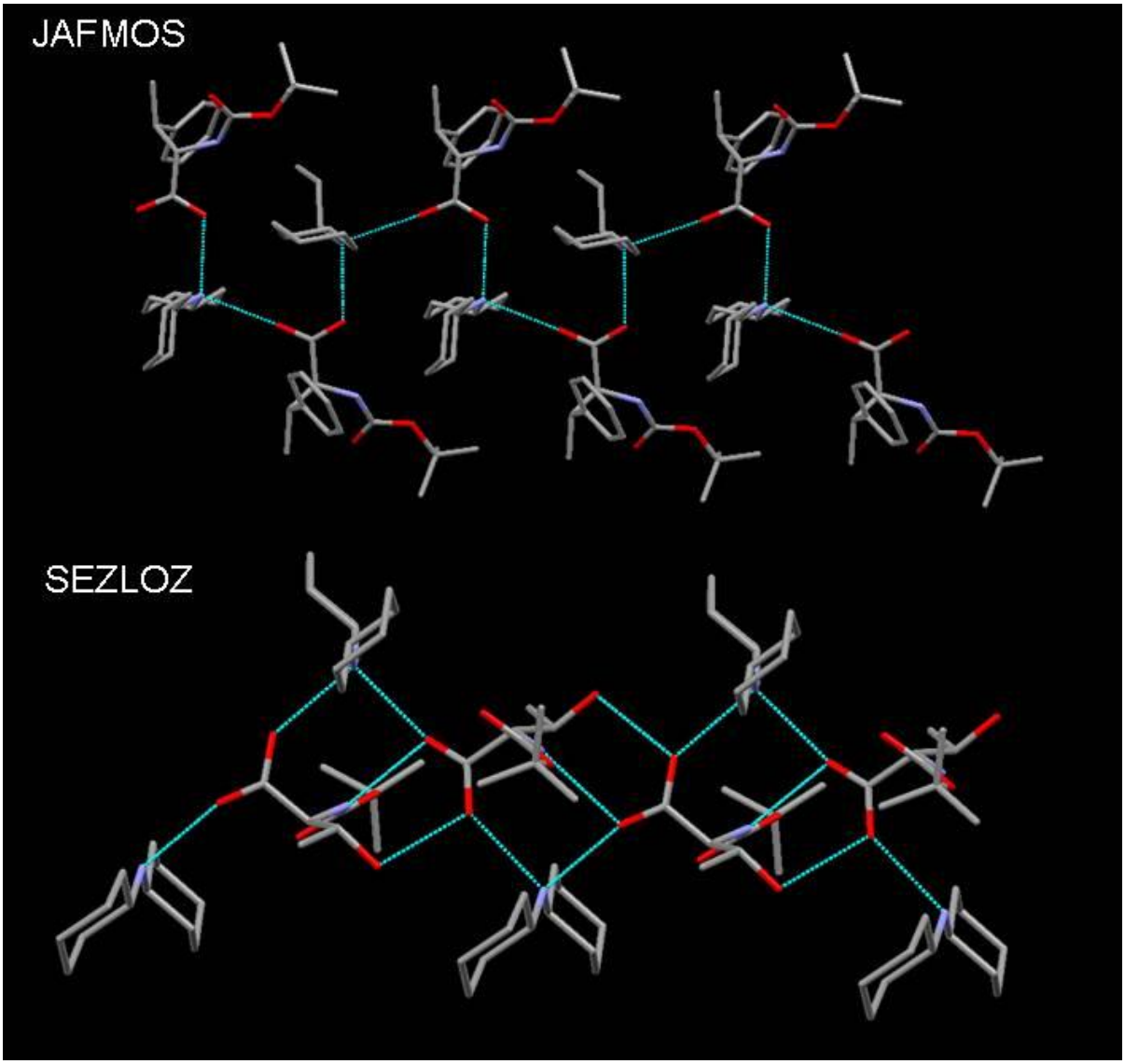

Figure S11 | Gel Sculpture Preparation

Preparation of Gel Sculpture

1. Soap
2. Soap Sculpture
3. Before addition of hot wax
4. After addition of hot wax
5. Template: after washing out the soap in hard H_2O
6. Gel formed inside the template
7. Taking out of gel sculpture from wax template
8. Final gel sculpture: 'Mother & Child'